SLAC-PUB-3199
August 1983
(I)

THE CENTRAL DRIFT CHAMBER FOR THE MARK III DETECTOR AT SPEAR*

J. Roehrig[a)], K. Einsweiler, D. Hutchinson, E. McNerney, A. Odian,
K. Skarpaas, Y. Unno[b)], F. Villa

Stanford Linear Accelerator Center
Stanford, California 94305

F. Grancagnolo[c)], W. Rowe, A. Seiden

University of California, Santa Cruz
Santa Cruz, California 95064

R. Baltrusaitis[d)], J. Hauser, J. Richman, J.J. Russell[e)]

California Institute of Technology
Pasadena, California 91125

G. Blaylock, J. Thaler, W. Wisniewski

University of Illinois
Urbana, Illinois 61801

(Submitted to Nuclear Instruments and Methods)

ABSTRACT

A large cylindrical drift chamber has been constructed for the MARK III detector at SPEAR. The inner layer has a high density of sense wires for the measurement of kinks, vees, and dE/dx. The outer layers have a cell design with three sense wires, giving uniform drift behavior and left/right ambiguity resolution within a cell. The chamber has both current division and stereo layers for longitudinal position measurement.

---

* Work supported by the Department of Energy, contract DE-AC03-76SF00515.

Present addresses:
a) Xonics Imaging, 601 West California, Sunnyvale, CA 94086
b) Natl. Lab. for High Energy Physics, Ibaraki-Sen, 305 Japan
c) EP Division, CERN, 1211 Geneva 23, Switzerland
d) Physics Department, Univ. of Utah, Salt Lake City, UT 84112
e) Xonics Imaging, 601 West California, Sunnyvale, CA 94086

I. INTRODUCTION

The MARK III detector is a third generation, general purpose detector designed to operate at the SPEAR e^+e^- storage ring at SLAC. Although charged particle multiplicities, which average about four, are not unmanageable at this energy, good detection efficiency and particle identification are essential for the study of exclusive decay processes.

The central detection device for tracking and momentum measurement of charged particles is a large cylindrical drift chamber with a rather novel design, shown in Figure 1. The chamber contains two regions: an inner region with a high density of sense wires, and a larger outer region with six discrete layers. The inner region consists of 32 axial cells, each containing 13 tungsten wires radially for a total of 416 wires. Each of these cells also has two stainless steel[1] guard wires which measure position along the beam direction (subsequently called the z coordinate) near the innermost and the outermost radius of this region. Of the 13 tungsten wires in a cell, the central wire is not read out, reducing the number of measurements to 12 per cell. In the outer region all cells are nearly identical in size and design, each containing three staggered sense wires. The outer region consists of four axial and two stereo angle layers, containing a total of 528 cells and 1,584 sense wires. The z-measurements are obtained using the stereo layers together with charge division[2] in three of the axial layers.

In this paper we will describe the geometrical and electrical parameters of our design, the choice and properties of our gas, and some details of construction and electronics. Finally, we will describe the performance of the chamber during the first year of running at SPEAR.

II. DESIGN DESCRIPTION

The drift chamber is a cylindrical annulus with 2.28 m outer diameter and 0.28 m inner diameter as shown in Figure 2. The inner gas barrier supports a small drift chamber containing four layers of sense wires, collectively called "layer 1", which will be described elsewhere.

The indented region allows space for the compensating magnets and supports the innermost, high density layer, layer 2. This layer consists of 32 cells of the "jet chamber" type configuration[3] (Fig. 3). The high density of sense wires in this region was chosen primarily to make possible the reconstruction of kinked tracks and vees from decays, and secondly to allow the possibility of measurement of dE/dx for e-π and low momentum K-π separation. The outer layers, referred to as layers 3-8, have three staggered sense wires per cell as shown in Figure 4. Layer N has N × 16 cells at a radius of N × 13.45 cm, hence all cells in the outer layers are approximately equal in size: 5.28 cm full width and 4 cm high. The dimensions and other relevant information are shown in Figures 3 and 4 and summarized in Table 1.

III. ELECTRIC STRUCTURE

The structure of the drift cells in layers 3 through 8 was designed to:

1. provide immediate resolution of the left/right ambiguity,
2. contain as constant an electric field as possible to simplify the space-time relation,
3. provide z coordinate measurement by current division as well as by stereo.

The negative voltages on the field wires of these cells increase radially in order to maintain equal gains on the sense wires. However, since the lateral dimension at the cell center is equal in all layers, the central field wire has the same voltage, 4,300 volts for all layers. All sense wires and guard wires are at ground potential. These voltages result in a gain of approximately 2×10^5 for layers three through eight using a gas mixture of 89% Argon, 10% CO_2, 1% Methane.

Constant gain of all sense wires is desired independent of boundary conditions such as presence of neighboring layers, presence of the gas barrier at the inner and outer radius, etc. The inner hexcell tube and the inner surface of the outer panels are maintained at a voltage approximately half the typical field wire high voltage, to prevent deterioration of efficiency on the wires close to these boundaries.

The relative simplicity of the cell design featuring one field wire per sense wire has one drawback, which is a rather large field at the surface of the field wire (see Section V). The sense wires are 20 μm diameter gold plated tungsten. The guard wires, on which current division is used, are resistive stainless steel. The signal on the guard wires is induced by the sense wires. The magnitude of the induced pulse is approximately 20% of that on the sense wires. In order not to have gas gain, their diameter is rather large, 57 μm. In practice the two guard wires are joined at the ends, doubling the pulse height, and halving the resistance to about 700Ω.

Figure 5 shows the equipotential surfaces in a cell of one of the outer layers (layer 5). Figure 6 shows the corresponding electron trajectories from a charged track. It also shows that the radial sensitive area is about 1 cm for each sense wire. The field is remarkably uniform over approximately 90% of the cell volume, with a value of 800 volts/cm. The field increases only in the last few mm near a wire.

IV. CONSTRUCTION

The end plates for layer two were constructed from 2.54 cm thick G-10 plates with Cu cladding on the inner surface. The holes were precision drilled on a numerically controlled milling machine, but later measurements revealed the precision to be about 100 μm, somewhat worse than originally specified. The layer two end plate is supported 27 cm inside of the end plates of the outer layers by a cylindrical tube 0.5 cm thick and 71 cm in diameter.

The outer layers are supported by end plates made from 7.62 cm thick aluminum honeycomb. A row of five wires pass through oversize radial slots, which were cut out of the hexcell with a routing machine guided by a template. To avoid any possibility of breakdown with nearby high voltage wires, the inner surfaces of the slots were covered with 10 mil thick mylar tubes. The actual wire position within slots are determined by precision holes drilled in 16 pie-shaped G-10 index plates 0.8 mm thick that are glued on top of the aluminum faceplates of the hexcell. Figure 7 shows the feedthroughs, which are made from injection molded Valox 710. Notable features of their design are: large, robust construction to avoid high voltage breakdown and the absence of any metal parts. The hole in the nose section is 250 μm in diameter, but the wire position is made more precise by insuring that it is always on one side of this hole. This is done by off-centering the brass spades to which the wires are soldered (see Fig. 7). The actual wire position accuracy is determined by the widest diameter of the "nose" which rests on the precision holes in the index plates on the inner surface of the chamber. This widest diameter is approximately 25 μm smaller than the nominal hole diameter. Concentricity and roundness of the feedthrough holes were checked optically, and are within ± 25 μm. Positioning of the holes within a G-10 index plate were checked to be better than ± 25 μm. Relative positioning between index plates was measured with a specially made measuring machine using telescopes mounted on precision x-y optical movements and are known to better than 25 μm. The position of any wire on the outer layers is therefore known to approximately 50 μm.

The inner radius of the chamber is closed off with a 2 meter long tube made from phenolic clad paper hexcell 0.95 cm thick, with inner and outer skins made from 50 μm mylar sheets with 8 μm aluminum cladding. The aluminum clad surface inside the drift chamber is maintained at 2,000 volts while that on the outside is held at ground. The thickness of the surface is only 1.7×10^{-3} radiation lengths. The outer radius of the chamber is closed off by six 6.25 mm thick curved aluminum plates, joined to form a cylinder, which support the load of the wires in the chamber. These plates also have an insulated aluminum clad mylar inner skin maintained at 2,000 volts.

The gas seal is made in the outer surface of the aluminum plates by a 0.3 cm thick layer of fiberglass covered with epoxy. The gas seal on the end plate containing the feedthroughs was made by placing the entire endplate in a horizontal position, and pouring on a layer of Dow-Corning Sylguard approximately 0.5 cm thick. In the wet state the Sylguard is only slightly more viscous than water, allowing penetration into all crevices. After setting, the Sylguard has roughly the texture of hardened silicone rubber.

Because the chamber has three types of wires with widely different mechanical properties, stringing the chamber was a fairly complex procedure. The 175 μm diameter field wires, made from Cu-Be, required a tension of 500 grams, which corresponds to a stretching of 3 cm. Sense wires, which were 20 μm gold plated tungsten required 50 grams of tension (equivalent to a stretch of only 1 cm over a length of 2.4 m), while the 57 μm stainless steel guard wires required 100 grams. In order to accommodate these three different tensions, the chamber was wired in the following way: beginning with the innermost circumference and working out, Cu-Be field wires were strung from one end to the other and soldered on both ends with only a nominal tension of 10 grams. Sense wires were soldered on only one end, brought through the other end with about 15 cm extra length, and attached to hooks made of heavy gauge wire. Stainless steel guard wires were crimped on one end, and attached to small hooks on the other end similar to the sense wires. These hooks were then attached to about 15 cm lengths of elastic, which were then hung on connectors about 30 cm from the surface of the chamber. After all wires were fastened in this way, the end plates were separated an additional 3 cm, bringing the chamber to its final length of 2.34 m, and bringing the Cu-Be field wires to their final tension of 500 grams. The sense and guard wires were then individually taken off their elastic supports and soldered or crimped to the feedthroughs with their nominal tension of 50 and 100 grams, respectively. Since the sense wires contribute less than 10% to the total force on the endplates, the deformation of the endplates is almost totally produced by the field wires, making prestressing unnecessary.

The wires were cleaned after this stringing operation by blowing on them with an industrial blower (similar to a paint sprayer) filled with isopropyl alcohol. The outer aluminum panels and inner hexcell tube were then installed to close the entire drift chamber volume.

V. SELECTION OF GAS MIXTURE

The chamber uses a 89% Argon, 10% CO_2, 1% Methane mixture[4] supplied in premixed tube trailers. The gas flow system is open to the atmosphere and uses only simple filters to remove large contaminants. No cleaning or recirculation of the gas is performed. The flow rate is maintained at 20 SCFH, which keeps the overpressure in the chamber at approximately 2.5 mm H_2O. The oxygen level at this flow rate has been measured to be approximately 125 ppm. During running a fraction of the input and exhaust gas is passed through a proportional tube to monitor changes in pulse height due to contaminants or changes in atmospheric conditions. Figure 8 shows a plot of (pulse height out)/(pulse height in) vs flow rate, and the O_2 concentration of the output. For normalization, the O_2 concentration of the input was measured to be 50 ppm.

Though many gases were considered, the final choice was made for a gas that did not grow "whiskers". The field at the field wires in the chamber is rather large, approximately 30 kV/cm, placing a serious burden on the stability of the gas. The original selection of gas, 70% Argon, 30% propane, was made on the basis of good drift properties, small sensitivity to concentration changes, and good behavior for dE/dx. This mixture worked well in a number of prototypes, and failed in the real chamber because of the growth of carbon filaments, or "whiskers". This phenomenon appears to be initiated by breakdown or corona on a field wire, due to some defect. After this filament growth was duplicated in a number of prototypes, whiskers were also successfully grown in prototypes using a number of common gases, such as 50/50 Ar/Ethane, and 80/20 Ar/Methane. The whisker growth always required some initial "catastrophy" or corona to initiate the process. No whisker growth was observed with the gas finally selected, 89% Ar/10% CO_2/1% Methane.

Figure 9 shows the measured drift velocity vs E field, showing saturation at a field of 800 V/cm. The width of the cells is 5.28 cm, making the maximum drift time approximately 550 ns, which is acceptable for the readout electronics.

VI. ELECTRONICS

Connections to the drift chamber are made using printed circuit cards mounted on the face of the chamber. These connections consist of the readout of the sense wires, the current division outputs, and a separate high voltage for each circumferencial ring of field wires. Connections to the outside of the detector for signal outputs are then accomplished with easily removable mass terminated coaxial cables which attach to the PC boards. The high voltage PC boards for the outer layers of the drift chamber feed five separate high voltages to a group of four cells per board. Each high voltage is bypassed by a 1 nF capacitor to ground and connected by current limiting 30 MΩ series resistors to the field wires. The local ground for the sense wires and field wires are physically very close, minimizing long inductive ground returns. In odd numbered layers (which use current division) the stainless steel guard wires are also connected to nearby PC boards, each one servicing 24 adjacent cells.

Layer two, designed to operate at a gain 1/10 that of the outer layers, and containing 12 sense wires per cell, had unique problems. The main one was simply the small signal size which required the use of preamplifiers. The best solution to the signal/noise problems was to mount the preamp directly on the chamber, within approximately 5 cm of its sense wire. The preamps for a whole cell are contained on one printed circuit board. A problem introduced by many sense wires per cell is the presence of pulses of opposite polarity, induced by neighboring wires. The preamplifier boards therefore contain a string of "cross-talk decoupling" resistors connecting each sense wire to its nearest and next nearest neighbors. The value of each resistor is chosen to compensate for the positive induced pulse. Limited space on the chamber required the use of a very compact amplifier design. The Plessy SL560C wide band, low noise amplifier was found to be suitable. The gain of the preamplifiers, times a factor of five due to impedance matching (350 Ω vs 70 Ω for the outer layers) results in a gain of approximately 80 at the chamber as compared to the outer layers.

The main discriminators and amplifiers are located in a shielded room (the alcove) some distance away from the detector. Signals are carried on 13.5 m long mass terminated 70 Ω cables to the discriminators. Those from the z and dE/dx wires are carried to amplifiers on 10 m long cables. This length of coaxial cable has approximately 1 nF capacitance, placing limits on z resolution due to noise. The discriminators used are LeCroy MVL 100's, mounted 48 per board. Large boards (1 meter long) are used to save packaging costs, but require careful attention to layout of circuits in order to avoid inductances in ground and power busses. Inputs to all discriminators contain differentiation with time constants of approximately 75 ns. One therefore expects minimal problems due to ground loops between alcove and detector which would result in low frequency pickup. Thresholds at the chamber for layers 3-8 are 500 μV (into 70Ω), and 200 μV (into 350Ω) for layer two. Amplifiers for current division and dE/dx have low noise common base inputs and emitter follower pairs to drive the output.

The noise environment (determining thresholds) at the discriminators is dominated by two sources: a) non-beam related pickup in the alcove from nearby oscillating channels which were eventually repaired and b) beam related pickup. It was found that the outside of the beam pipe had a current caused by the beam's image charge escaping at breaks (ceramic windows) in the beam pipe. Shielding was put wherever possible and cable loops at the face of the chamber were minimized. The noise at the amplifier input is on the order of 10 fC for an integration time of 550 ns. Because of the long integration time, the electronics is more sensitive to low frequency components of noise. The noise is consistent with the value of the capacitance of the 10 m cable from the chamber to amplifier. All outputs of discriminators and amplifiers are differential, taken through 18 m twisted pair cable to the next higher level of electronics.

The event trigger is based primarily on information from the drift chamber[5]. The elements of the trigger are organized into a primary, secondary, and tertiary trigger which uses layers 1, 2, 3, and 5 to identify charged particle trajectories coming from the interaction region in coincidence with the beam crossing. Circles are found in the plane perpendicular to the beam line and sine curves in the longitudinal plane using the time and current division information provided by the drift chamber. Because one relies entirely on the drift chamber for event recognition, it is important that it be efficient. The efficiency achieved is about 97% per cell.

Timing information is recorded using multi-hit time to amplitude converters (MTAC's).[6] Signals derived from the beam crossing serve as a common start input to start the ramps in the MTAC's. The ramps are stopped by: a) a wire hit, b) the late stop pulse for events that passed primary level trigger but have no wire hit, c) the next reset pulse in the event of no primary trigger. A signal proportional to the difference between the start and stop in case (a) thus provides the time information. Provision has been made for up to four hits in each MTAC channel.

Multi-hit sample and hold electronics (MSHAM's)[7] are used to store pulse heights for current division and dE/dx. Although four bins for storage in principle are available per input, only the first bin, whose extent is the maximum possible drift time, is used. All analogue outputs from two CAMAC crates of MTAC's (or MSHAM's) are digitized by one ADC (the BADC).[8]

To convert the MTAC amplitudes into drift times a calibration system is essential. The functional form used to convert from BADC channel number to time is a quadratic. The parameters of the quadratic are determined in brief calibration runs taken about three times per day and are loaded into the BADC for data taking. Residuals are typically 1 ns (50 μm in space) for the quadratic fit. In the calibration procedure a time marker is used to generate delays that are integral multiples of 11.16 ns (one of the SPEAR RF frequencies), and set able by the VAX 11/780 online computer. The discriminators are then pulsed using the chosen delay. The part of the MTAC ramp parameterized is from 80 ns to 640 ns, avoiding early and late parts of the ramp, which are less linear. The calibration system has been crucial as a diagnostic tool for the electronics. "Unfittable" channels, which generally indicate dead or oscillating MVL 100's, are monitored by the calibration program. Figure 10 shows a schematic of the electronics for a wire in layer 2.

VII. USE OF WIRE INFORMATION

The drift chamber cell structure is designed so that a large amount of information about tracks and cell behavior is available prior to track reconstruction. In the outer layers this is based on the fact that there are three closely spaced position measurements. A straight line element (local tangent to a track) is described in terms of two parameters, thus leaving one constraint which can be used to solve the left-right ambiguity. For a triplet of wires, alternately staggered by $\pm\ \delta$ (see Figure 4), the quantity calculated is:

$$\Delta = v_{\mathrm{drift}} \left[(t1 + t3)/2 - t2\right],$$

where t1, t2, t3 are the measured times for a track passing through the cell. This quantity is double peaked, with peaks centered at $\pm\ 2\delta$, where the sign gives the side of the cell traversed. The left-right ambiguity can thus be locally resolved provided that $4\delta >>$ measurement error on Δ, which is $\sigma_\Delta = \sqrt{(3/2)}\sigma_x$, where σ_x is the spatial precision for each measurement. In our case, including electrostatic deflections, $4\delta = 2$ mm while $\sigma_\Delta = .25$ mm, allowing easy separation. Figure 11 shows a plot of Δ for all hits in layer 5 of the chamber. The region between the peaks comes from tracks crossing the cell center line. These can also be left-right sorted by generalizing Δ to consider this possibility.

An examination of Δ on a cell by cell basis allows one to make several important quality checks. 1) If one calls Δ^+ and Δ^- the positions of the two peaks, then their separation, $\Delta^+ - \Delta^-$, provides a measure of the mean electrostatic deflection of the three wires. Using this technique one can find wires which were not tensioned correctly and, in addition, measure the correction to the "ideal" wire position due to electrostatic deflections. 2) $\Delta^+ + \Delta^-$ should be centered at zero. An offset most likely implies an incorrect time pedestal for one or more of the wires involved.

The use of wire triplets has several features which are very useful for pattern recognition. The Δ check allows the elimination of bad points at an early stage in the pattern recognition. Having passed this check, a triplet of hits provides not only a local position but also a local tangent to the track. For tracks coming from the e^+e^- intersection region, this allows an immediate calculation of the track parameters R, ϕ_0 (radius of curvature and azimuth at origin) from: $R = 1/2 \text{ sqrt } (\rho^2 + (d\rho/d\phi)^2)$, $\phi_0 = \phi - \sin^{-1}(\rho/2R)$ where ρ, ϕ are the cylindrical coordinates measured and $d\rho/d\phi$ is the local tangent.

Track finding is done initially in the (ρ,ϕ) projection which contains 28 of the 34 wire planes available. The stereo hits (triplets in two layers) are then searched for possible matches. The chamber geometry allows approximately seven possible cells in the stereo layers for any given track in the (ρ,ϕ) projection. The current division measurement achieves an accuracy of about 1% of a wire length, or about 2 cm σ in z. This is approximately an order of magnitude worse than the stereo precision and therefore this information is mainly useful for very steep tracks, as a check on the stereo information and for pattern recognition.

The twelve signals resulting from a track passing through layer two are used for both timing and pulse height measurement. The timing information is handled similarly to that of the other layers. In this case we have more wires, each with smaller stagger, with which to resolve the left-right ambiguity after which layer 2 gives an independent track segment. The pulse height measurement is achieved by integrating the amplified signal falling within a one microsecond gate. After the tracking code has identified a track passing through layer two, these pulse height measurements are matched to the track in order to provide a maximum of twelve 1 cm samples of ionization for particle identification.

A number of corrections are required before the raw pulse height measurements become a reliable representation of ionization. These include gain and pedestal corrections for the electronics, corrections for pressure and temperature fluctuations, correction for a dependence on arrival time of the signal and correction for a dependence on the angle of the track through the cell.

The calibration for the dE/dx system is done offline by comparing the pulse height distribution for each channel with a standard distribution. The standard distribution is obtained experimentally from a large sample of elastic e^+e^- events. This is adequate to describe the general shape of the single pulse distribution and allow comparisons between channels. Relative gains and pedestals between channels can then be estimated to a few percent, which is sufficient for our purposes.

Gas pressure and temperature are monitored by a barometer and thermocouples. Theory predicts that the dependence of pulse height on pressure and temperature should be roughly:

$$PH = PH_0 * \exp(-A*P/T) \qquad [A > 0]$$

Though primary ionization should increase with gas density, the negative exponent occurs because increased density in the avalanche region results in lower average collision energy and reduced gain. For our gas at atmospheric pressure, a 1% increase in pressure corresponds to about a 6.7% decrease in pulse height.

A dependence of pulse height on drift time arises from two notable sources. A typical pulse after shaping has a rise time of about 80 nanoseconds, a crossover point after about 600 nanoseconds and a small overshoot rising slowly back to zero. The effect of a fixed 1 microsecond integration gate is to truncate more of the overshoot for longer drift times (up to about 400 nanoseconds) thereby making the pulse height measurement larger. For drift times longer than 400 nanoseconds, part of the positive pulse is truncated and the measurement reduces again. In addition, slight changes in the electric field across the cell make for different collection lengths depending on drift time. In particular, the stagger of the wires causes a difference between the two sides of a single cell. Because of the variation of cell size in layer two, these two effects combine in a unique way for each of the 12 wire layers, causing a typical variation in pulse height of 3-5 percent. A quadratic expression for each side of each wire layer is used to correct for the net drift time dependence. Pulses which come from tracks passing through the edge of the cell ("crossovers") are not used.

Because pulse height measurements are matched to a previously identified track, it is easy to sum them and divide by the path length through the cell to get a measure of dE/dx. However, even after correction for path length, there remains a correlation of pulse height with the angle the track makes with the wire as shown in Figure 12. This effect is attributed to space charge resulting from the avalanche process. As the ionization is collected, relatively immobile positive ions from the avalanche process form a cloud surrounding the signal wire. Subsequent avalanches may take place in a region of reduced electric field and therefore reduced gain. For tracks which pass perpendicular to the wire all of the ionization is deposited at the same point on the wire and this effect is maximal, whereas for tracks passing at small angles to the wire the ionization is spread out along the wire and the space charge effect is smaller. In principle this effect may depend on parameters other than the track dip angle, such as the time distribution of the avalanches, fluctuations in primary ionization and track angle in the ρ-ϕ plane. Some effort has been spent trying to find these dependences but no significant trends are apparent in our data. The drift chamber geometry gives a solid angle = 83% of 4π over which one has tracking with full stereo information. Going out to layer three one has 93% of 4π with good tracking with at least the cruder current division z information. Over this full range, layer two gives dE/dx information for particle identification to complement the 80% of 4π coverage of the TOF scintillation counters.

VIII. PERFORMANCE

The overall performance of the drift chamber has been studied using mainly J/ψ decays. Certain questions such as the proper operating voltage and measurement of plateau curves were determined with sources and cosmic rays. The significance of the triplet distribution, Δ, was discussed in the previous section. The important points of performance that are contained in these distributions will be summarized here. The width of the peaks gives an initial resolution of 250 μm. Note that this "resolution" integrates over all z's, and over all cells, and therefore represents in some sense the resolution one might expect without special cell by cell or z dependent corrections. By binning this distribution in z, the electrostatic deflection of the wires ($\Delta^+ - \Delta^-$) can be measured, as shown in Figure 13. This figure shows that the mean sagitta is about 200 μm, which is consistent with a wire tension of 50 grams.

Optimum performance requires knowledge of both the drift velocity and the t_0 for each wire, where t_0 is the earliest possible measured time (corresponding to a track passing through the sense wire). The t_0's for each channel are obtained from the data using the shape of the leading edge of the time spectrum and stored in a disk file for input to the tracking program. Obtaining the best resolution for the chamber required the determination of further constants which specify the space-time relationship. These quantities, illustrated in Figure 14, are an average velocity for the nearly radial drift near the sense wires, the Lorentz angle and constant drift velocity for the central 70% of the cell, and a quadratic correction near the field wires. Separate parameters were calculated for both the left and right sides of each sense wire using an iterative least squares procedure minimizing the residuals for a large number of tracks in the detector.

The final resolution achieved is approximately 220 μm per measurement for layers 3-8 and 300 μm per measurement in layer 2. Pulse height corrections reduce the latter number to 250 μm. Track parameters, without a vertex constrained fit, are determined to a typical precision of:

$$\Delta p/p = 0.015\sqrt{1+p^2}$$
$$\Delta\phi = .002$$
$$\Delta\tan\lambda = .011$$

where the momentum p is measured in GeV/c, ϕ is the azimuthal angle and λ is the dip angle. The first term in $\Delta p/p$ comes from multiple scattering.

Figure 15 shows the distribution of momenta measured for di-muon events at the J/ψ mass. The gaussian superimposed has a σ = 45 MeV/c. Figure 16 shows the measured z distribution for a charge division measurement in layer 5, after subtraction of the z coordinate predicted by the more accurate stereo measurements. The standard deviation corresponds to a precision of about 1.5 cm.

The results of our dE/dx measurements show that layer two is useful for e-π separation and low momentum K-π separation. Figure 17 shows the single pulse distribution for a sample of muons from $\psi \rightarrow \mu^+\mu^-$. The full width for this distribution is roughly 100% of the peak value. Because the distribution is shewed toward large pulse heights, a truncation procedure is applied. The pulse heights for each track are ordered, and the highest, which have suffered the largest fluctuations, are discarded, while the lower pulse heights, containing the maximum information, are retained. It was found that the optimum resolution for tracks having all 12 measurements was obtained by averaging the lowest 9 values. However, the resolution does not increase substantially as long as anywhere from 6 to 10 of the lowest pulse height measurements are used. Figure 18 shows the mean of the lowest 9 pulse heights when 12 measurements are available. The superimposed Gaussian has a sigma of 15% of the peak value. This resolution allows good K-π separation up to about 500 MeV (figure 19). The Fermi plateau for this gas is 175% of the minimum-ionizing value. For a 15% resolution, this results in the e-π separation plotted in Figure 20. The solid curves in Figures 19 and 20 are calculated from the Landau form for the most probable energy loss, modified for the density effect as determined by Sternheimer & Peierls.[9] For our gas this is:

$$E_{mp} = N/\beta^2 \, [8.226 + 2\,\ln(\gamma) - \beta^2 - \delta]$$

where

$$\delta = 0 \qquad [X < 2.0]$$

$$\delta = 4.606*(X-2.61) + 0.3518*(4.0-X)**3 \qquad [2.0 < X < 4.0]$$

$$\delta = 4.606*(X-2.61) \qquad [4.0 < X]$$

with $X = \log_{10}(\Upsilon)$ and N adjusted to agree with the data.

REFERENCES

1. Trademark STABLOHM 800 wire, California Fine Wire Company.
2. V. Radeka, IEEE Trans. Nucl. Sci. NS-21 (1974) 51.
3. W. Farr et al., Nucl. Inst. and Meth 156 (1978) 283.
4. We first learned of this gas from the members of the High Resolution Spectrometer experiment at SLAC.
5. J. Thaler et al., IEEE Trans. Nucl. Sci. NS-30 (1982) 236.
6. H. Kang, IEEE Trans. Nucl. Sci. NS-28 (1981).
7. D. Bernstein, IEEE Trans. Nucl. Sci. NS-28 (1981).
8. H. Brafmann et al., IEEE Trans. Nucl. Sci. NS-25 (1978) 692.
9. R.M. Sternheimer and R.F. Peierls, Phys. Rev. B11 (1971) 3681.

TABLE 1

Drift Chamber Specifications

Inner Radius	14.47 cm
Outer Radius	114.26 cm

Layer 2:

Number of Cells	32
Wire Length	177.8 cm

15 wires with 1 cm spacing

Innermost wire #1	17.45 cm	radius
Outermost wire #15	31.45 cm	radius

Wires 1 and 15 are charge division wires of 57 μm diameter stainless steel

Wires 2-14 are sense wires of 20 μm diameter tungsten, however wire 8 is not used

Smallest cell half width is 1.81 cm (400 ns drift time)

Largest cell half width is 2.99 cm (600 ns drift time)

Alternate sense wires are displaced ± 150 μm

Layers 3-8:

Cells contain 5 wires, #1 and #5 are guard and charge division wires of 57 μm diameter stainless steel, #2-#4 are sense wires of 20 μm tungsten. Wire length is 233.7 cm.

Field wires are 175 μm CuBe

Radial position of center wire (#3) is 13.45 × N cm, where N is the number of the layer

The number of cells is 16 × N

Stereo layers	#4	7.7° stereo angle
	#6	-9.0° stereo angle

Charge division on layers 3, 5, and 7

Typical half cell width is 2.64 cm (550 ns drift time)

Staggering is ± 400 μm

FIGURE CAPTIONS

1. Section of drift chamber endface showing the wire pattern in the chamber. Large solid circles are field wires, small solid circles are sense wires, small open circles are guard wires. Layers 4 and 6 are stereo layers. Induced signals on the guard wires for layers 2, 3, 5, 7 are used for charge division.
2. Section of drift chamber. Dotted regions are wire layers 3 through 8.
3. One cell of layer 2.
4. Typical cell in an outer layer.
5. Equipotential lines in a cell of an outer layer of the chamber.
6. Typical drift patterns in the chamber showing the uniform collection region for each sense wire.
7. Chamber feedthrough showing long plastic section, nose section for positioning, and brass spade for soldering and electrical connection.
8. Chamber gain and O_2 contamination as a function of gas flow rate.
9. Drift velocity versus electric field for gas used in chamber.
10. Schematic for the electronics for layer 2 of the drift chamber.
11. Distribution of $\Delta = v_{drift}((t1+t3)/2 - t2)$, where t1, t2, t3 are the drift times in a cell. The two peaks correspond to tracks passing on the left and right sides of the cell.
12. Plot of ln(PH) vs cos(θ) showing the space charge effect. Pulse heights have already been corrected for path length.
13. Electrostatic deflection of a sense wire versus longitudinal position. Curve is a parabolic fit.
14. Relation of drift distance measured (dotted line) and distance along a line through sense wire and tilted at Lorentz angle. Circles indicate approximate region of radial drift. Space-time relation requires specification of average velocity inside circle, velocity in linear drift region, and a quadratic correction near the field wires (not shown). MARK III chamber has $a = 1$cm, $\theta = 17°$.
15. Measured momenta for muons produced at the J/ψ resonance. Superimposed curve has a $\sigma = 45$ MeV/c.

16. Residual in longitudinal position for charge division in layer 5. The predicted position is gotten from the stereo measurements and the residual is plotted as a fraction of the wire length.
17. Single pulse height distribution for muons from $\psi \rightarrow \mu^+\mu^-$.
18. Truncated mean (lowest 9 of 12 pulse heights) for muons.
19. Demonstration of K-π separation. Solid curves are Landau form for the most probable energy loss.
20. Calculated K-π and e-π separation in units of pion sigma. The Landau/Sternheimer formula has been used assuming a 15% resolution.

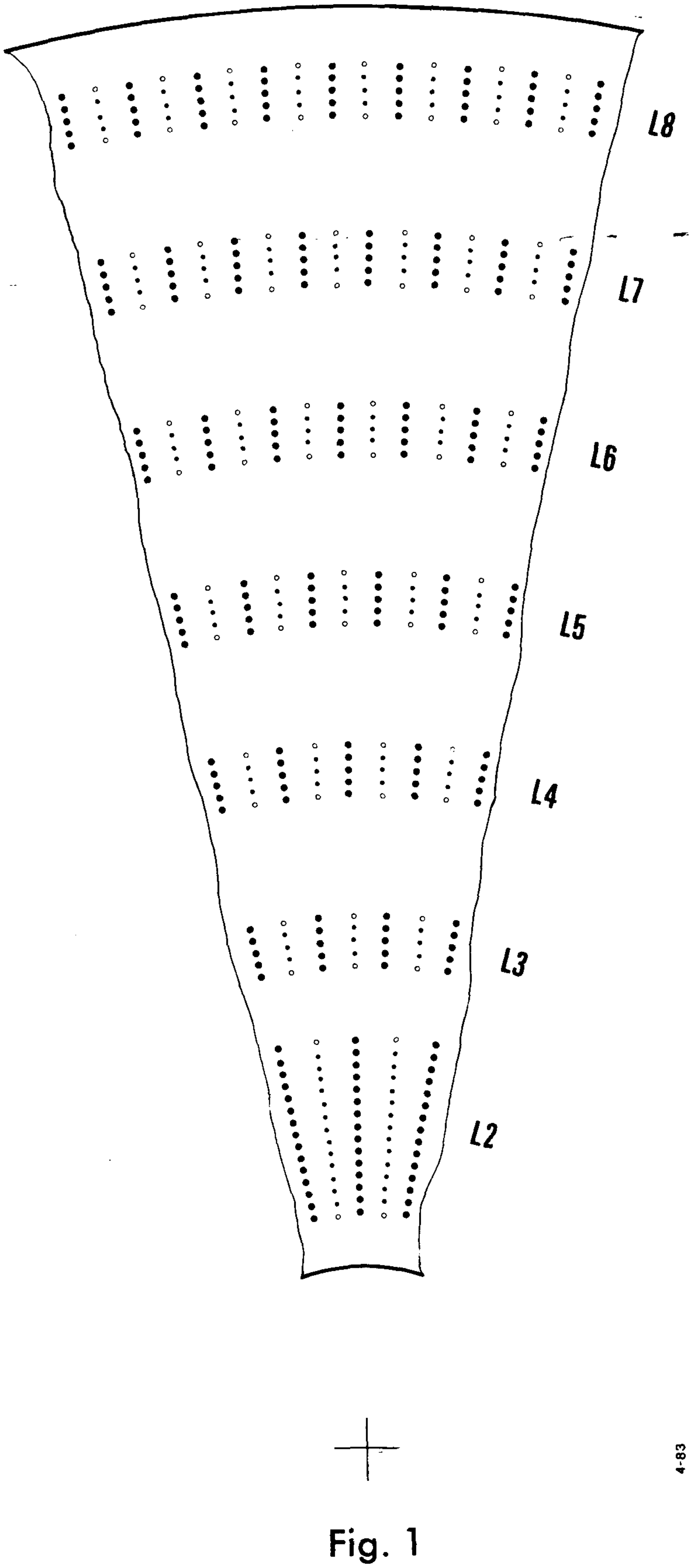

4-83
4430D11

Fig. 1

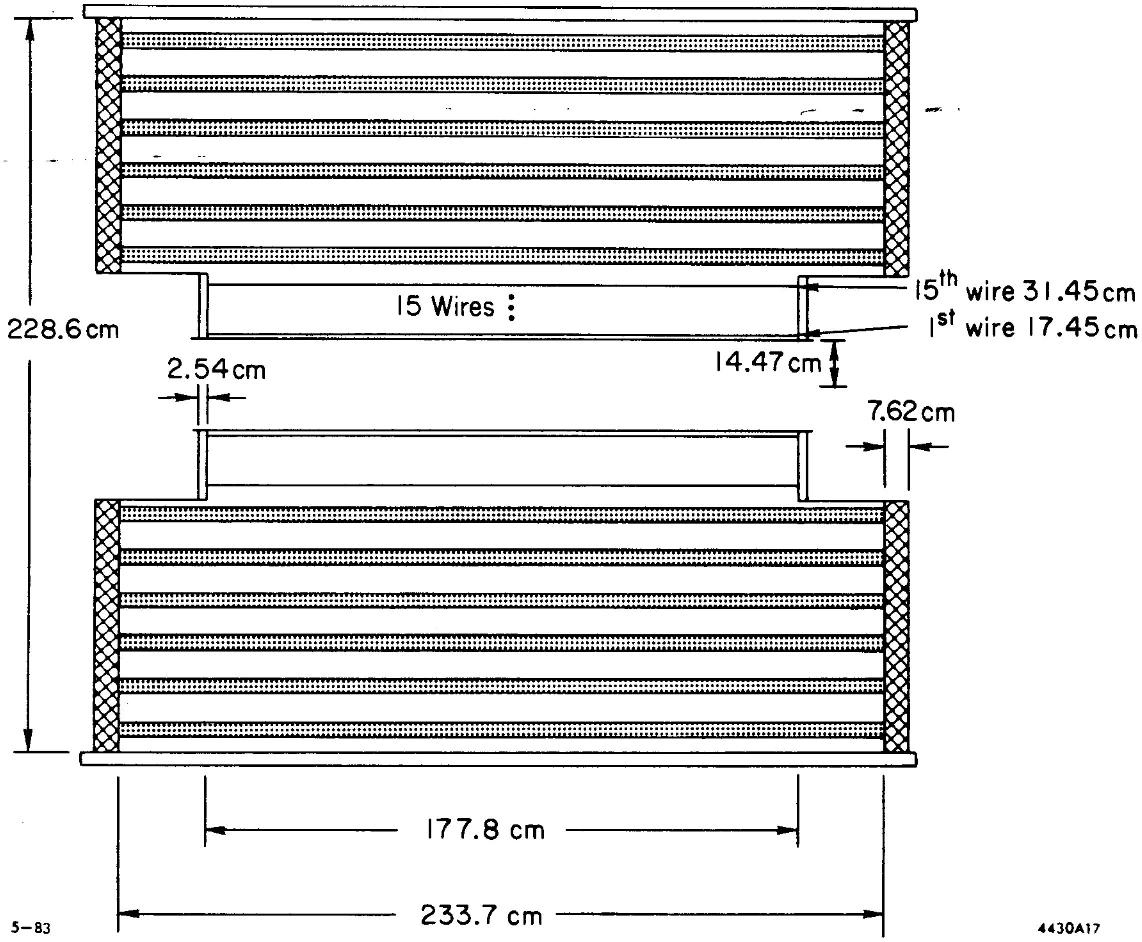

228.6 cm
15 Wires
15th wire 31.45 cm
1st wire 17.45 cm
14.47 cm
2.54 cm
7.62 cm
177.8 cm
233.7 cm
5-83
4430A17

Fig. 2

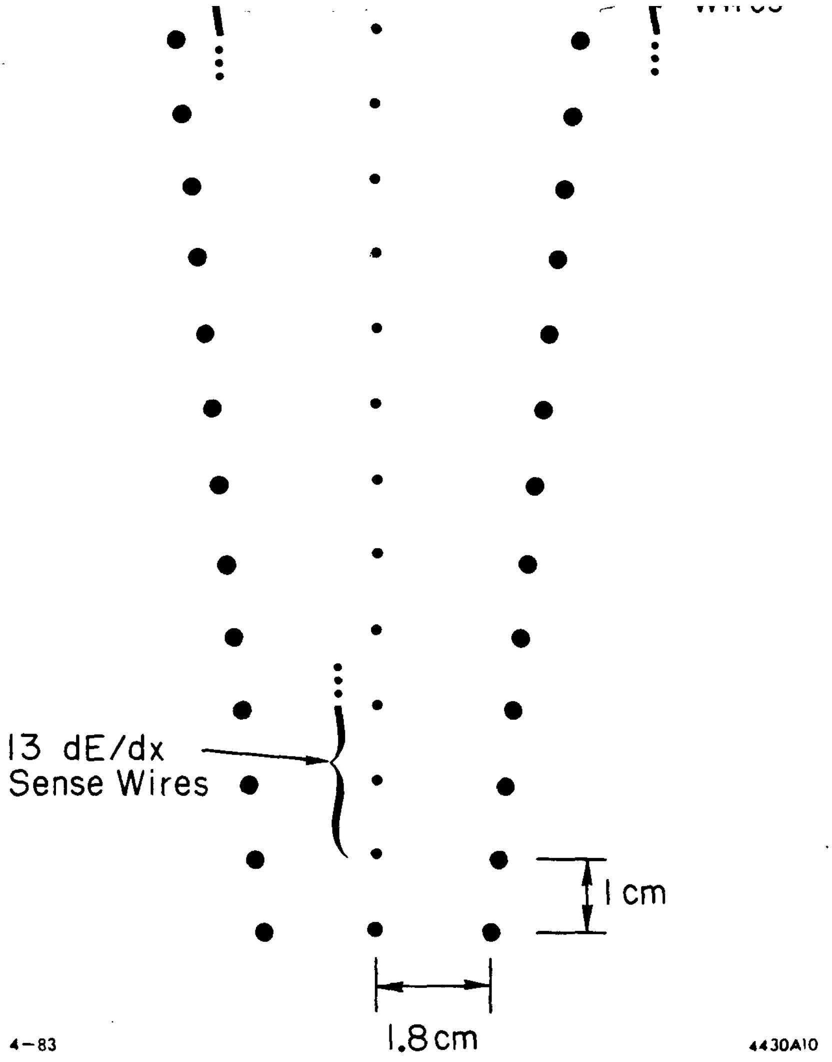

Fig. 3

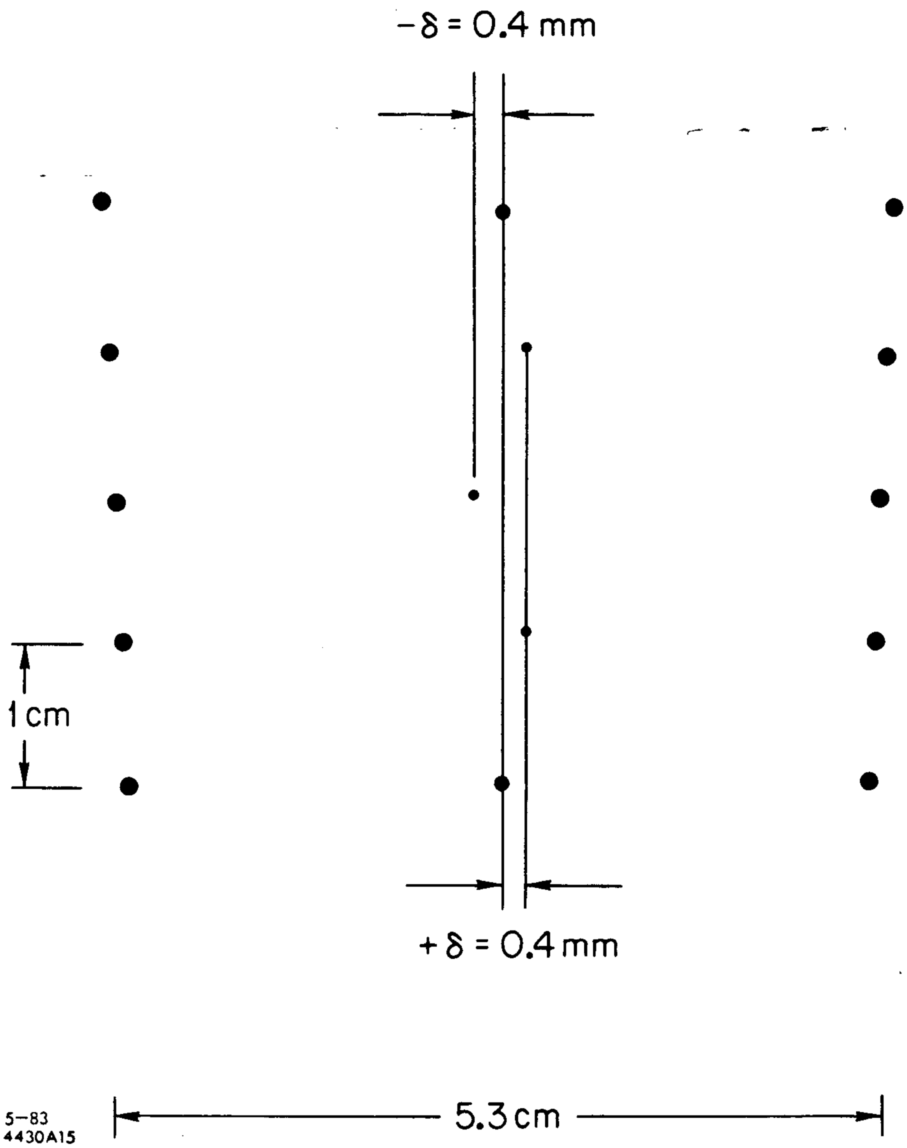

Fig. 4

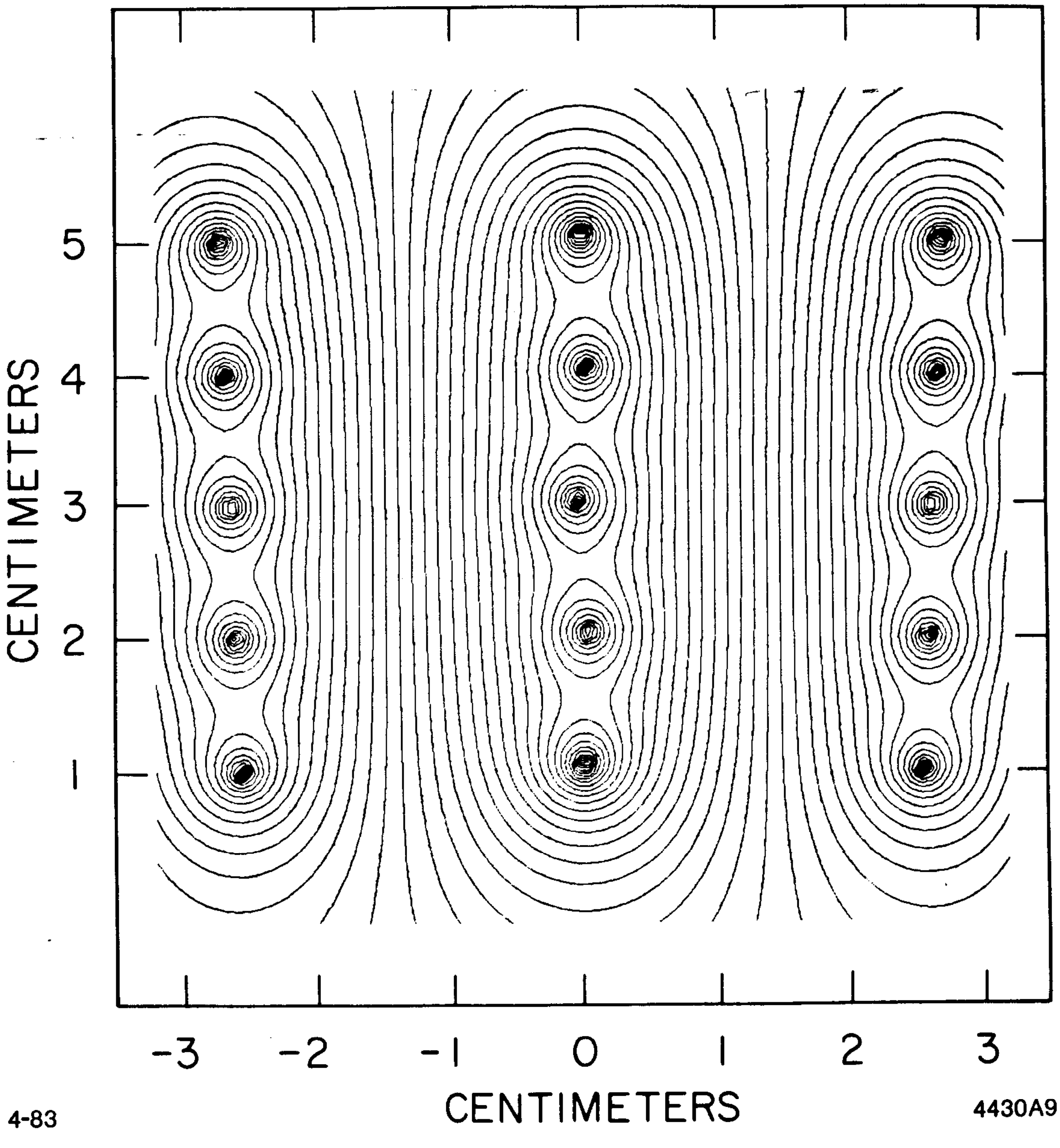

Fig. 5

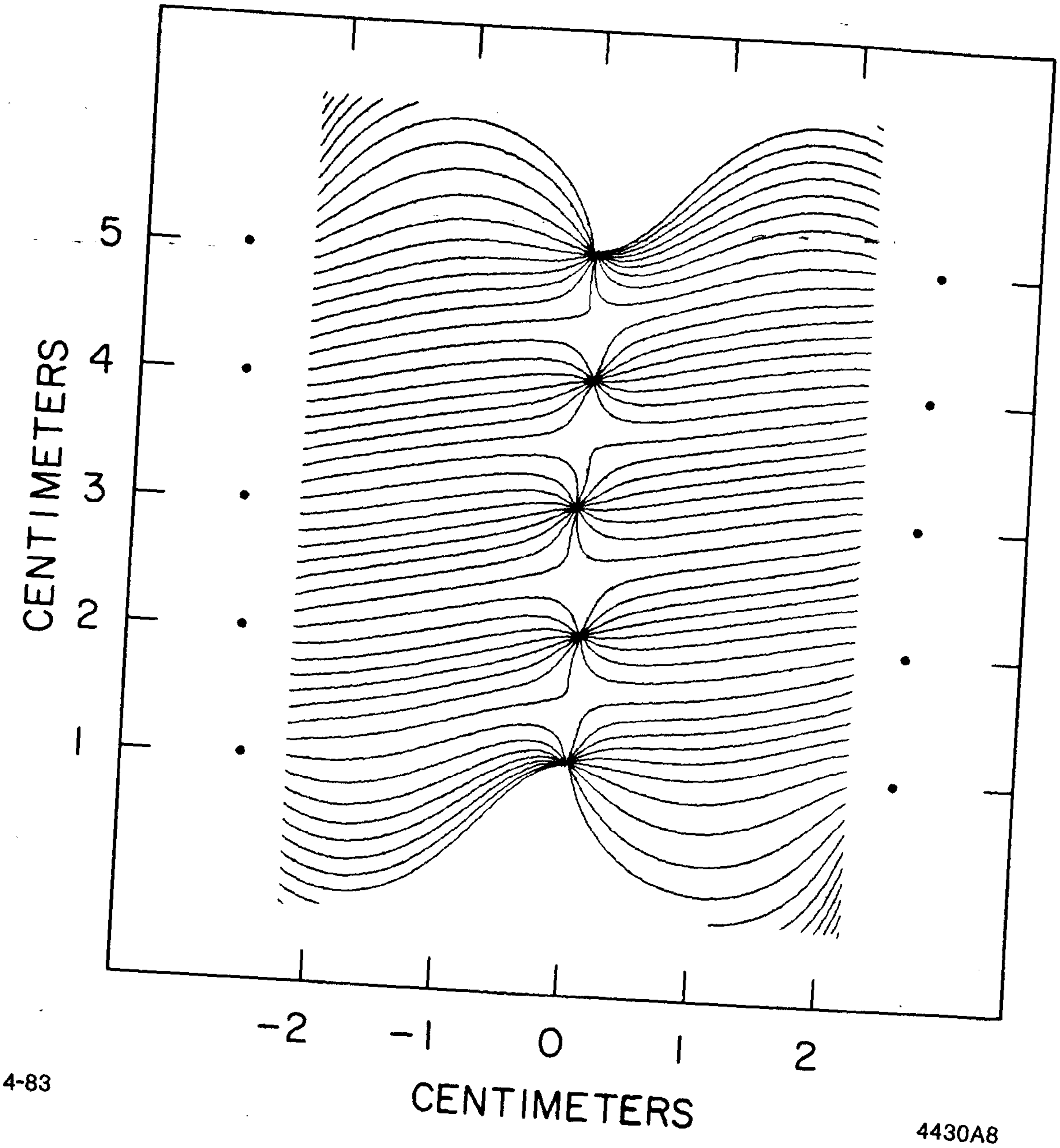

Fig. 6

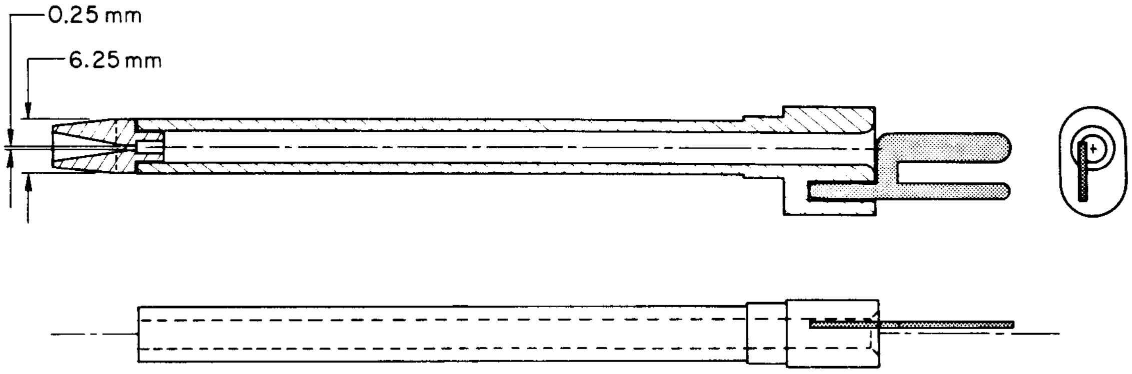

1-83

4430B7

Fig. 7

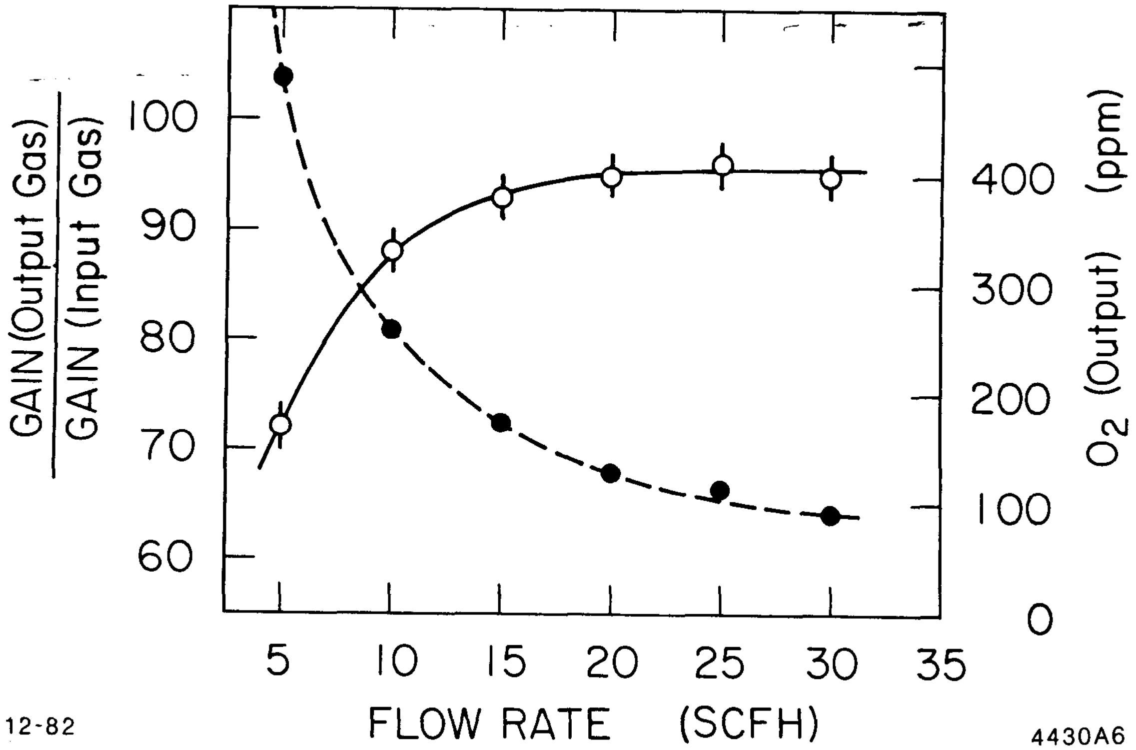GAIN (Output Gas) / GAIN (Input Gas)
100
90
80
70
60
400
300
200
100
0
O₂ (Output) (ppm)
5
10
15
20
25
30
35
FLOW RATE (SCFH)
12-82
4430A6

Fig. 8

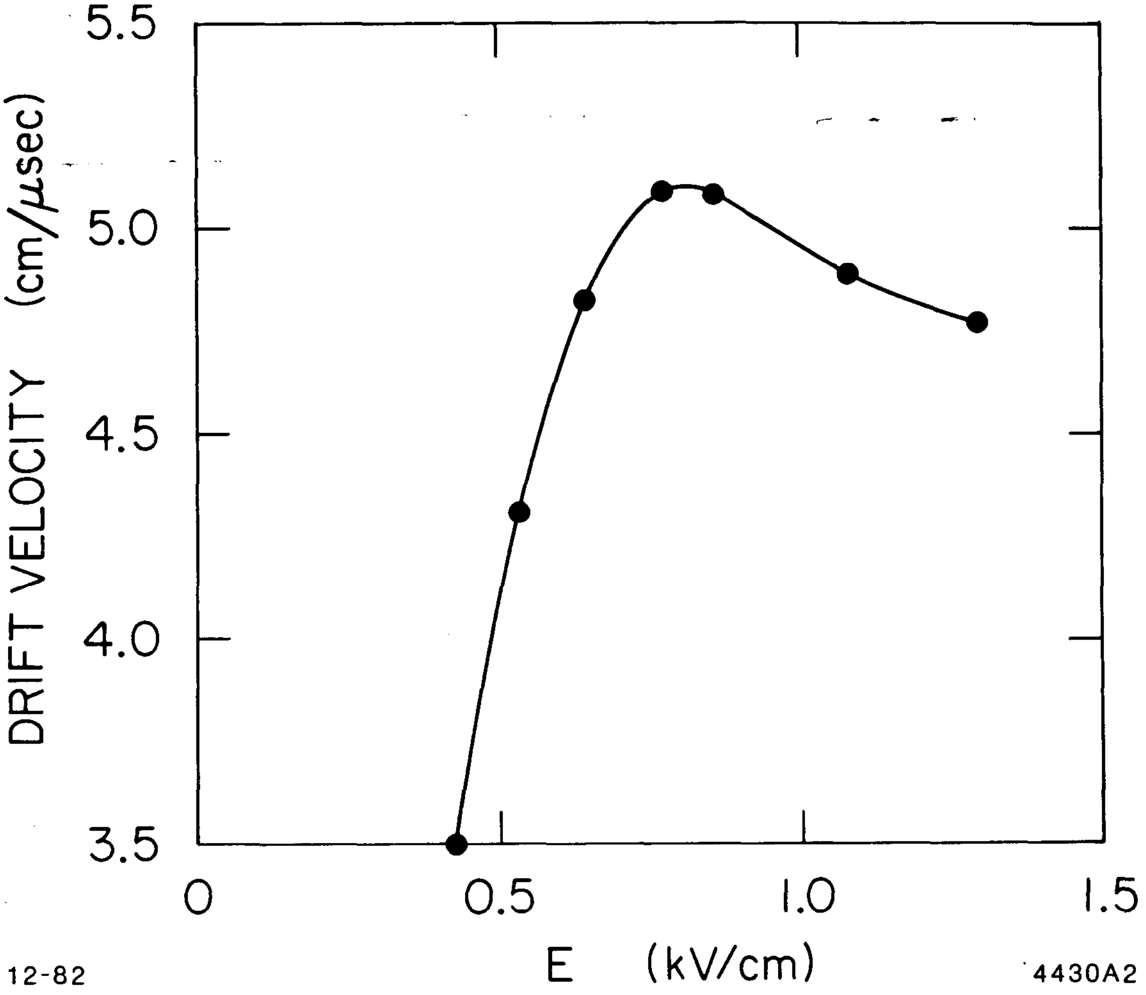
5.5
5.0
4.5
4.0
3.5
DRIFT VELOCITY (cm/μsec)
0
0.5
1.0
1.5
E (kV/cm)
12-82
4430A2

Fig. 9

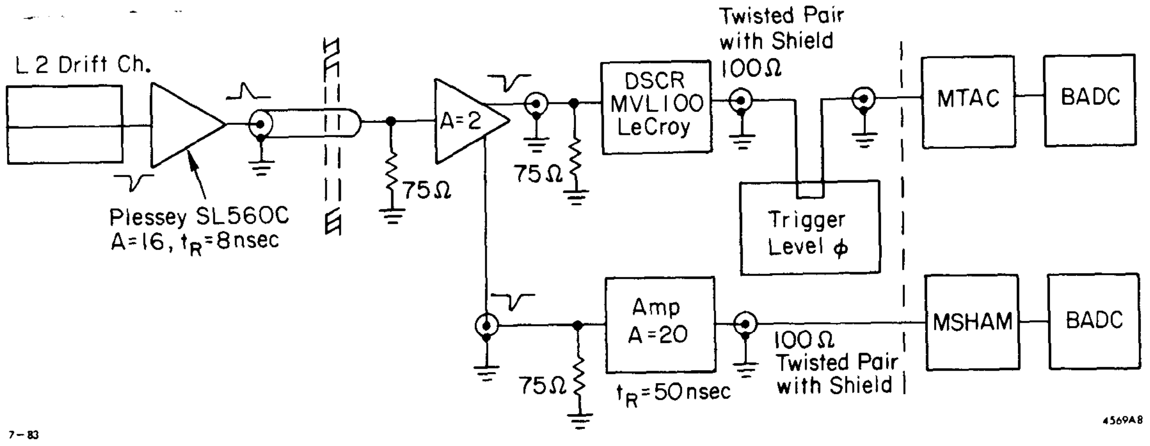L 2 Drift Ch.
Plessey SL560C
A=16, t_R=8nsec
75Ω
A=2
75Ω
DSCR
MVL100
LeCroy
Twisted Pair
with Shield
100Ω
Trigger
Level ϕ
MTAC
BADC
Amp
A=20
75Ω
t_R=50nsec
100Ω
Twisted Pair
with Shield
MSHAM
BADC
7-83
4569A8

Fig. 10

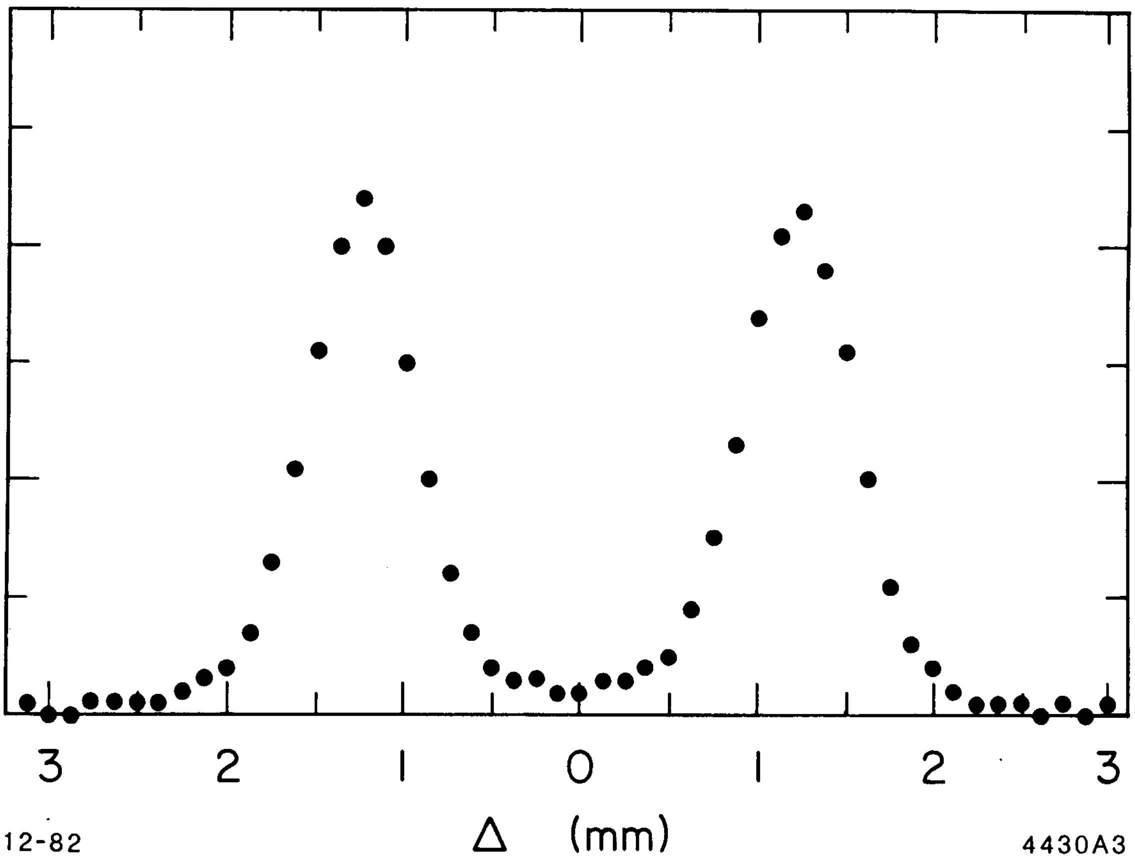

Fig. 11

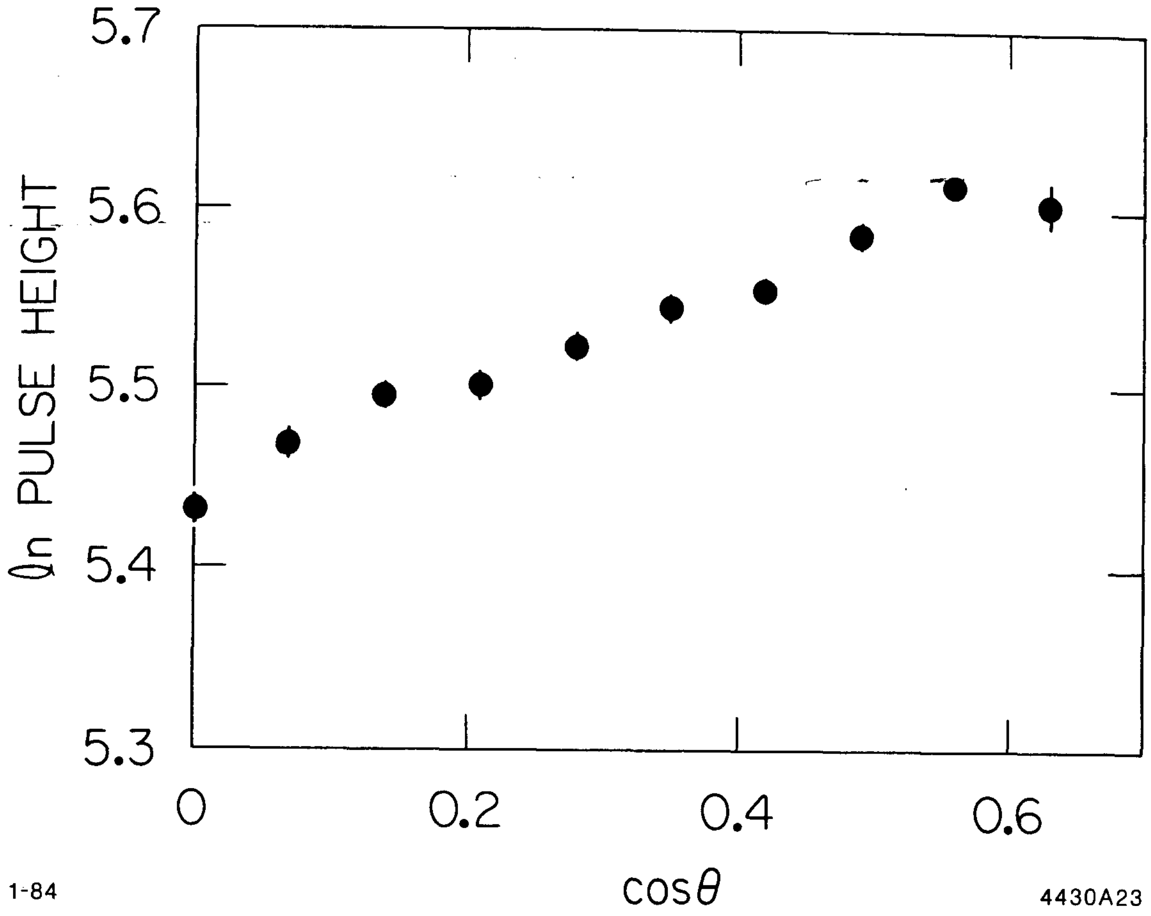

Fig. 12

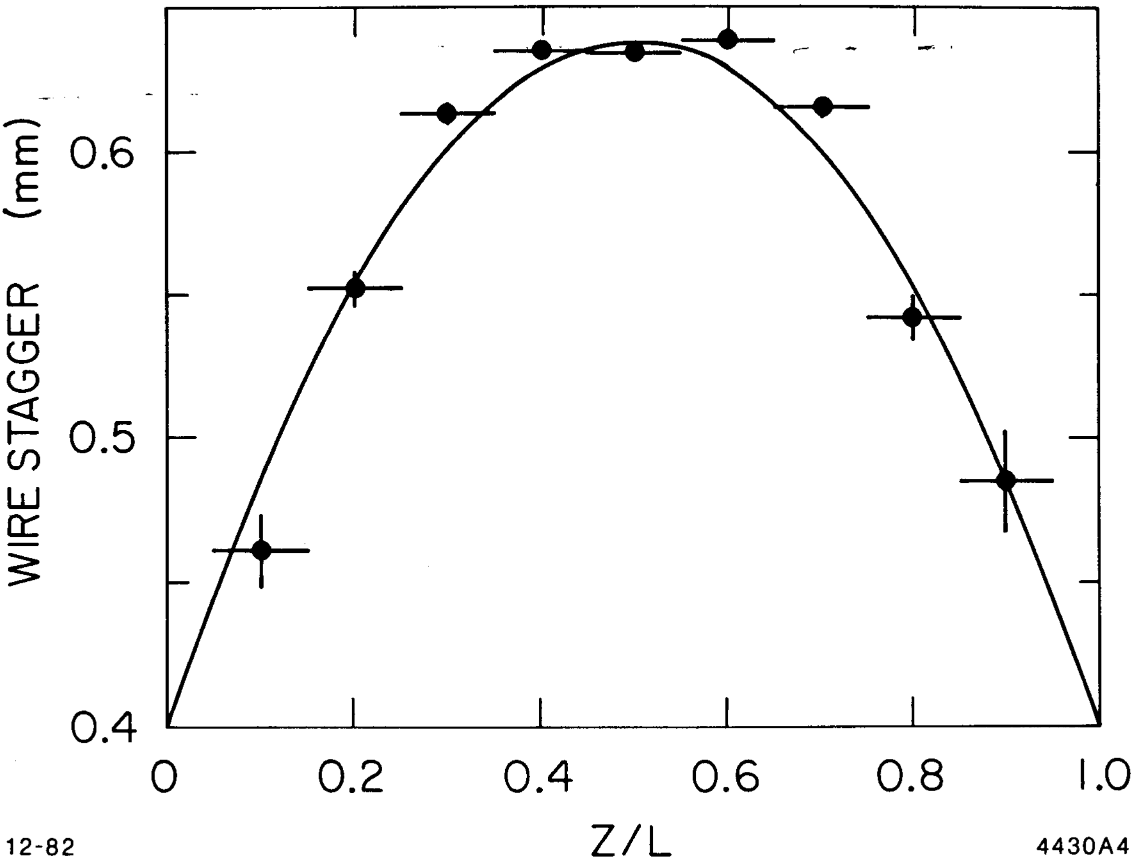

Fig. 13

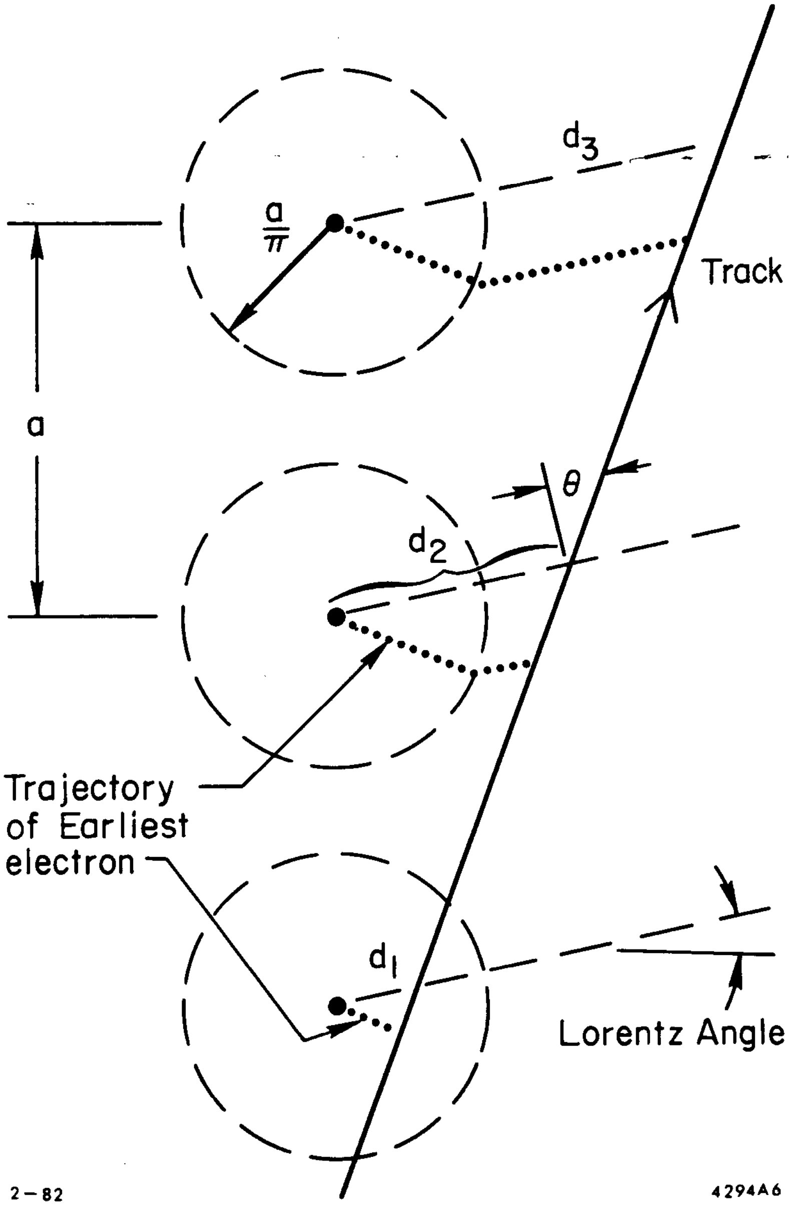

d_3
$\frac{a}{\pi}$
Track
a
θ
d_2
Trajectory of Earliest electron
d_1
Lorentz Angle
2-82
4294A6

Fig. 14

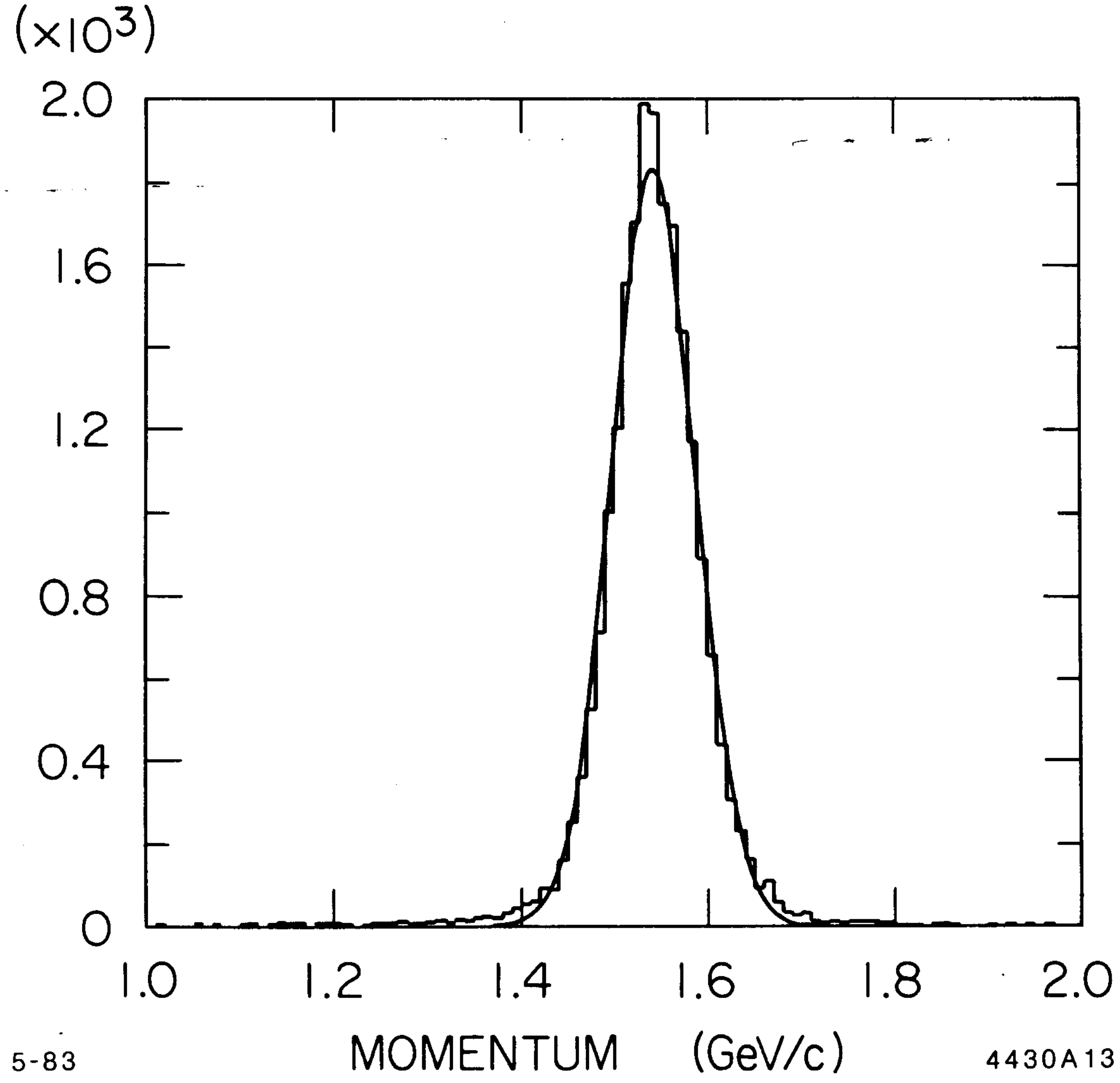

Fig. 15

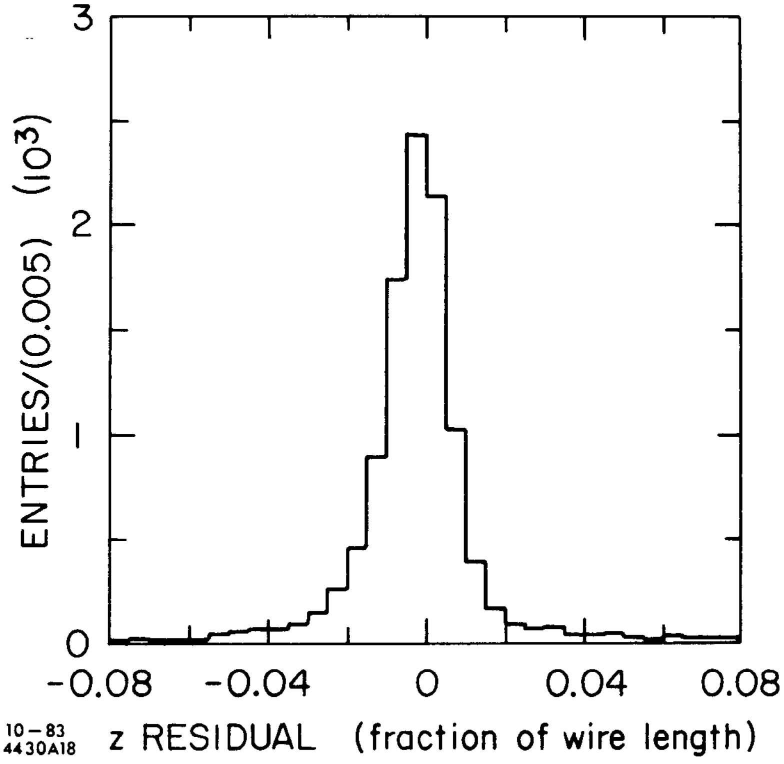
3
2
1
0
ENTRIES/(0.005) (10³)
-0.08
-0.04
0
0.04
0.08
10-83
4430A18
z RESIDUAL (fraction of wire length)

Fig. 16

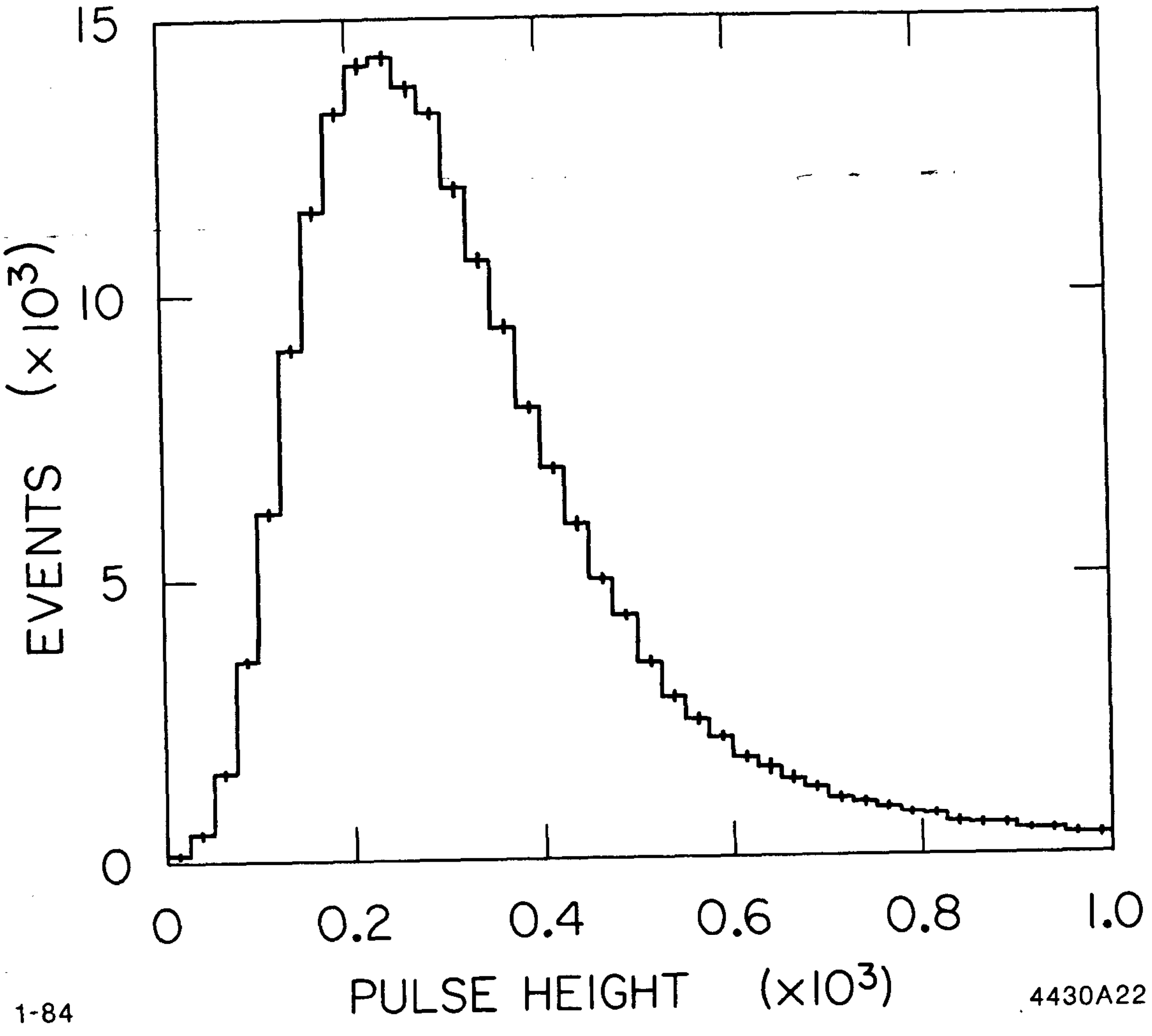
15
10
5
0
EVENTS (×10³)
0
0.2
0.4
0.6
0.8
1.0
PULSE HEIGHT (×10³)
1-84
4430A22

Fig. 17

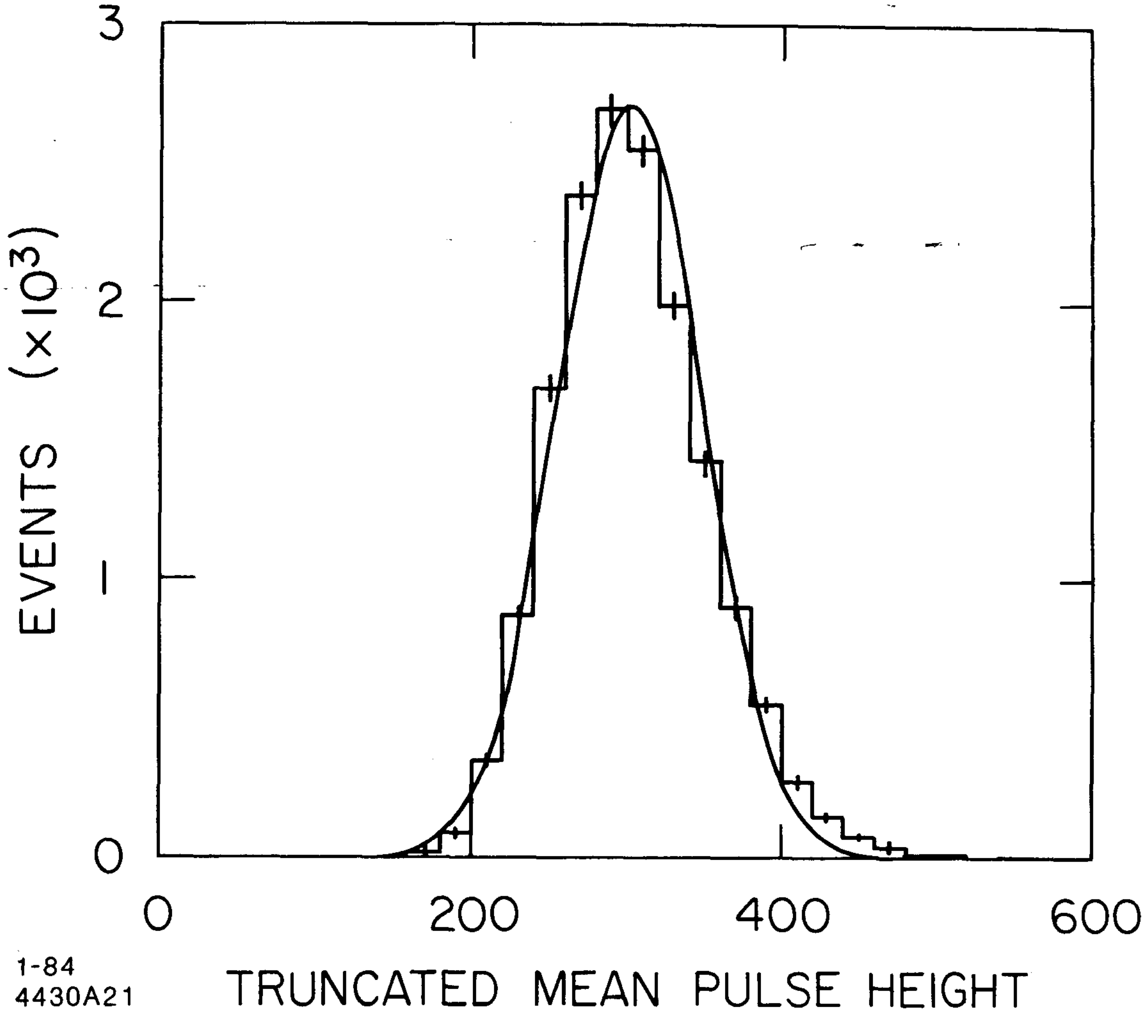
3
2
1
0
EVENTS (×10³)
0
200
400
600
TRUNCATED MEAN PULSE HEIGHT
1-84
4430A21

Fig. 18

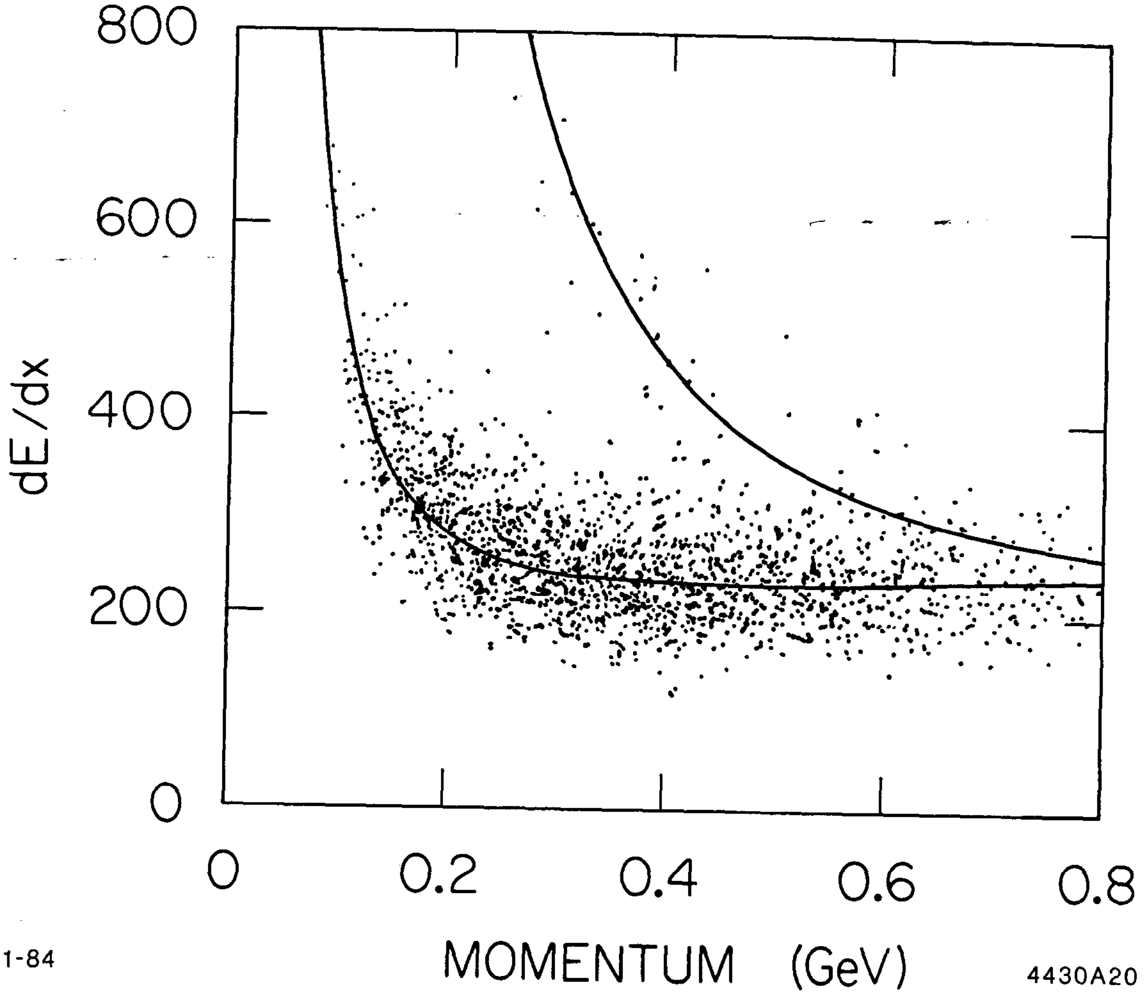

Fig. 19

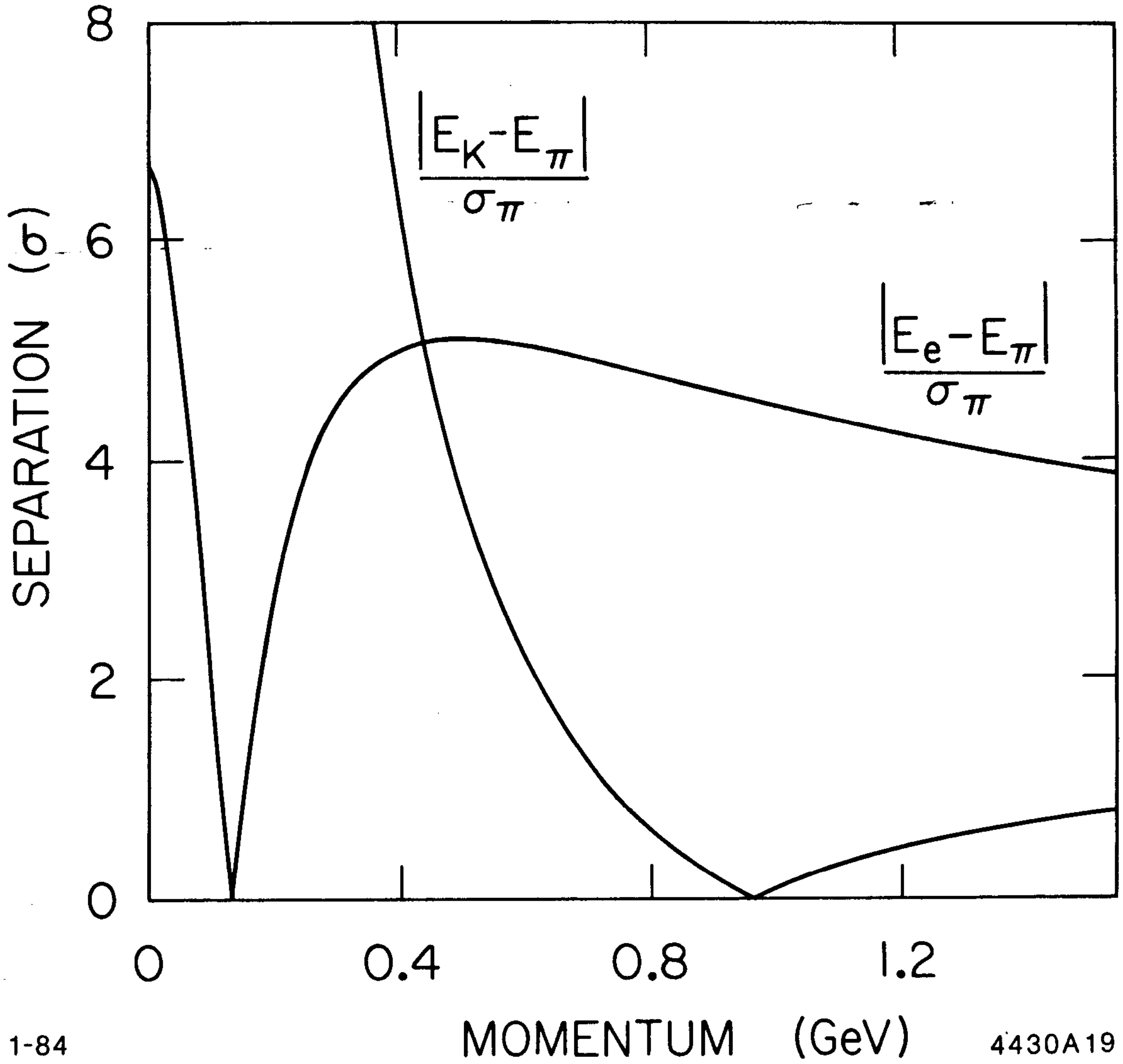
8
6
4
2
0
SEPARATION (σ)
0
0.4
0.8
1.2
MOMENTUM (GeV)
$\frac{|E_K - E_\pi|}{\sigma_\pi}$
$\frac{|E_e - E_\pi|}{\sigma_\pi}$
1-84
4430A19

Fig. 20